separations

MDPI

Article

Application of Bio-Based Activated Carbon from Cocoa Husk Waste for High-Efficiency Adsorption in Water Treatment

Daniela Angelova [1,*], Vesislava Toteva [1] and Georgi Georgiev [1,2]

[1] Department of Textile, Leather and Fuels, University of Chemical Technology and Metallurgy, 8 Kliment Ohridski Blvd., 1797 Sofia, Bulgaria; vesislava@uctm.edu (V.T.); georgiev@uctm.edu (G.G.)
[2] Institute of Organic Chemistry with Centre of Phytochemistry, Bulgarian Academy of Sciences, Acad. G. Bonchev Street, bl. 9, 1113 Sofia, Bulgaria
* Correspondence: daniela_angelova@uctm.edu

Abstract

This research presents the study of utilizing the cocoa husk biomass waste to obtain active carbon through carbonization method, followed by chemical–thermal activation. The activated carbon (CH) was characterized using BET, SEM–EDX, XPS, and Raman techniques. The obtained material showed a high specific surface area of 1661 $m^2 \cdot g^{-1}$, and XPS confirmed the presence of oxygen-containing surface functionalities. The adsorption of reactive dye Drimaren Red K-7B by CH was studied to assess the impact of the initial concentration in water solution, temperature, and contact time. The adsorbent achieved over 90% removal within three minutes at 40 °C. The experimental data for the adsorption of Drimaren Red K-7B using CH showed a good fit with the Dubinin–Radushkevich isotherm and a pseudo-second-order kinetic model. This research offers a promising approach for advancing the circular economy through the obtaining of eco-friendly adsorbents derived from biomass waste, exhibiting high initial adsorption efficiency and rapid uptake kinetics towards reactive dye.

Keywords: bio-based material; water purification; adsorption kinetics; reactive dye removal; thermodynamics; adsorption isotherms; cocoa bean husk

check for updates

Academic Editor: Xinhua Qi

Received: 31 July 2025
Revised: 1 October 2025
Accepted: 4 October 2025
Published: 10 October 2025

Citation: Angelova, D.; Toteva, V.; Georgiev, G. Application of Bio-Based Activated Carbon from Cocoa Husk Waste for High-Efficiency Adsorption in Water Treatment. *Separations* **2025**, *12*, 278. https://doi.org/10.3390/separations12100278

Copyright: © 2025 by the authors. Licensee MDPI, Basel, Switzerland. This article is an open access article distributed under the terms and conditions of the Creative Commons Attribution (CC BY) license (https://creativecommons.org/licenses/by/4.0/).

1. Introduction

Industrialization and rapid population growth have intensified water pollution challenges globally [1]. Around 80% of the world's wastewater—mostly untreated—enters rivers, lakes, and oceans, heightening the need for effective solutions [2].

Industrial sectors such as textiles, printing, leather, dyeing, polystyrene packaging, paper, food, and cosmetics significantly contribute to water pollution by discharging untreated wastewater contaminated with dyes into aquatic systems [3]. The release of such effluents poses serious risks to both human health and aquatic ecosystems. Consequently, implementing treatment before discharge is essential. The identification and optimization of wastewater treatment methods are of critical environmental importance. Currently, technologies employed for treating dye-contaminated wastewater include oxidation [4,5], ion exchange [6], coagulation [7], ozonation [8], filtration [9], biological methods [10], and adsorption [11–13].

Among the various techniques applied in the treatment of dye-laden wastewater, adsorption stands out as one of the most prevalent and efficient methods. Its popularity stems from the straightforward implementation process and cost-effectiveness in removing

diverse dye compounds from aqueous solutions [14,15]. Conventional adsorbents, typically derived from finite natural resources such as coal, peat, and petroleum-based byproducts, tend to be costly and demand frequent and complex regeneration procedures [16]. Because of such limitations, researchers are now directing attention to identifying alternative, low-cost, and environmentally sustainable sources for activated carbon production and other bio-based adsorbents for water purification [17,18]. In the pursuit of sustainable solutions for dye-contaminated wastewater, recent studies have increasingly focused on natural and biogenic materials as viable alternatives to conventional adsorbents [19,20]. Polysaccharide-based hydrogels derived from renewable sources such as chitosan, cellulose, and starch have demonstrated notable efficiency in capturing dye molecules, benefiting from their high density of functional groups and adaptable porous structures [21]. Complementary research on biogenic adsorbents obtained from plant biomass, algae, and microbial residues has shown that targeted chemical or thermal modifications can significantly enhance adsorption capacity and selectivity [22]. Furthermore, green materials including cellulose nanofibers, alginates, and lignin-based composites offer the dual advantage of biodegradability and tunable surface chemistry, enabling tailored interactions with specific dye classes [23]. These developments highlight a clear trend toward low-cost, eco-friendly, and high-performance materials, providing a relevant context for the cocoa husk-derived activated carbon explored in this work.

Building on these advances, agricultural and other biological wastes have gained traction as low-cost precursors for activated carbon production due to their abundance, renewability, and environmental benefits [24]. In this context, cocoa bean husks, an unexplored agro-industrial byproduct, have been identified as a promising precursor material. Through a combined carbonization and KOH activation process, the resulting material exhibits high porosity and a well-developed micro/mesoporous structure. The study combines the use of waste materials with testing and analysis, showing that the material's surface and pore structure make it highly effective and rapid in removing the dye Drimaren Red K-7B from water. Comprehensive kinetic, isotherm, and thermodynamic analyses further elucidate the adsorption mechanism, together forming the core of the study's original contribution to sustainable water purification technologies.

2. Materials and Methods

2.1. Materials

Cocoa husks obtained from local production were applied as starting material in the fabrication of activated carbon (CH). Chemicals used in this study were supplied by Sigma-Aldrich (St. Louis, MO, USA). Drimaren Red K-7B (Clariant, Basel, Switzerland) was used to prepare the aqueous solutions. Potassium hydroxide was used as a chemical activating agent.

2.2. Active Carbon Preparation

Due to their tendency to combust rapidly at elevated temperatures, cocoa husks require pretreatment to enhance their thermal stability prior to carbonization. In this work, the husks were mechanically compacted into pellets and subjected to pyrolysis at 400 °C for 30 min under a nitrogen atmosphere (flow rate: 150 mL·min^{-1}) with a heating rate of 2 °C min^{-1}. The obtained char was then impregnated with a 50 % KOH solution at a solid-to-liquid mass ratio of 1:1.2 (w/w) for 24 h, followed by drying to constant weight. This intermediate product underwent a second heat treatment at 800 °C for 60 min in nitrogen, using a heating rate of 5 °C min^{-1}. After activation, the material was rinsed with hydrochloric acid solution until the pH reached 5.5–6.0, then washed with distilled water to neutrality and finally oven-dried at 110 °C for 8 h.

2.3. Analysis

The characterization of the synthesized adsorbent included determination of its elemental composition, surface morphology, and porosity. Surface features and elemental distribution were examined using a SEM/FIB LYRA I XMU scanning electron microscope equipped with an energy-dispersive X-ray spectroscopy module (TESCAN, Brno, Czech Republic). The instrument operates within an accelerating voltage range of 200 V to 30 kV and offers a resolution of 3.5 nm at 30 kV. Prior to imaging, the specimen was coated with a thin gold layer via DC magnetron sputtering (Au K500×).

Textural parameters, including pore size distribution and total pore volume, were assessed by low-temperature nitrogen adsorption–desorption measurements conducted on a Quantachrome AUTOSORB iQ-C-MP-AG-AG NOVA 1200e analyzer (Quantachrome Instruments, Boynton Beach, FL, USA). Specific surface area values were obtained using the Brunauer–Emmett–Teller (BET) method.

Raman spectroscopy was performed on the CH sample using a Witec Alpha M300+ spectrometer (WITec GmbH, Ulm, Germany) fitted with a Nd:YAG laser (λ = 532 nm, maximum output 50 mW). Spectra were collected at 1 mW laser power, with an exposure time of 5 s, 50 accumulations, and a spectral range of 0–3800 cm^{-1}. The ratio of the D- to G-band intensities and areas (I_D/I_G), used to assess the degree of structural ordering in the carbon framework, was obtained using Witec Project 4.1 software.

Surface analyses of carbon and oxygen on the active carbon sample CH were performed by X-ray photoelectron spectroscopy (XPS, ESCALAB MkII) spectrometer at a base pressure in the analysis chamber of 5×10^{-10} mbar using an Al X-ray excitation source (Kα = 1486.6 eV).

2.4. Adsorption Studies

The adsorption studies were performed in batch mode, with a fixed volume of aqueous dye solution and continuous magnetic stirring at 300 rpm to ensure uniform mixing and effective contact between the adsorbent and adsorbate. The studied adsorbent, with a mass of 0.025 g, was added to 12.5 mL of aqueous Drimaren Red dye solution. To estimate the influence of the initial dye concentration, solutions ranging from 10 to 100 $mg \cdot L^{-1}$ were prepared. The effect of temperature on the adsorption process was assessed at 20 °C and 40 °C under the same experimental conditions.

The change in the dye concentration in the aqueous solutions was monitored with a UV-VIS spectrophotometer, recording absorption at a wavelength of λ = 548 nm with an ONDA UV-31 SCAN apparatus in the range 190–600 nm. The amount of adsorbed dye was calculated using the following equation:

$$q_e = \frac{(Co - Ce)V}{m} \quad (1)$$

where q_e is the adsorption capacity, $mg \cdot g^{-1}$; Co and Ce are the initial and equilibrium concentration of the dye, respectively, $mg \cdot L^{-1}$; m is the mass of the adsorbent, g, and V is the volume of the solution, L.

The percentage of dye removal D (decolorization) is calculated using the following relationship:

$$D(\%) = \frac{Co - Ce}{Co} 100 \quad (2)$$

The adsorption isotherm experiments were conducted using CH doses of 0.025 g in solutions with initial dye concentrations between 10 and 100 $mg \cdot L^{-1}$, at 20 °C, and a fixed contact time of 25 min. Kinetic measurements were carried out with the same

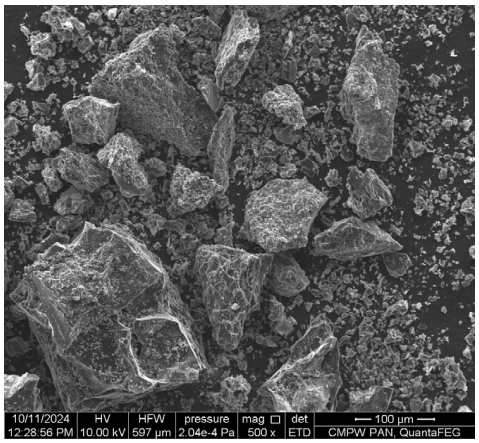
adsorbent dose and an initial dye concentration of 100 mg·L^{-1}, varying the contact time from 1 to 25 min, at two temperatures (20 °C and 40 °C). Thermodynamic parameters were derived from equilibrium data obtained at both temperatures.

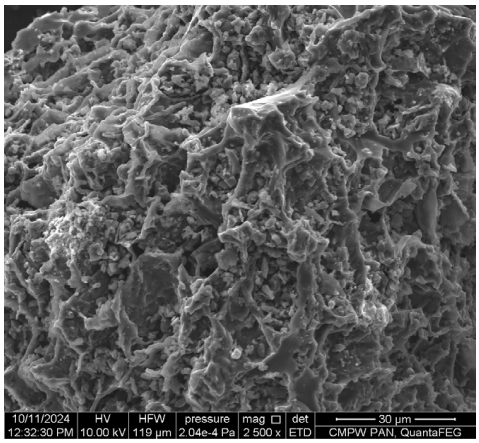
3. Results and Discussion

3.1. Morphological Analysis

The synthesized cocoa husk-derived activated carbon exhibits promising textural properties. These features suggest its strong potential as a high-efficiency bio-based adsorbent in water treatment applications.

Figure 1 presents the SEM micrographs of the CH sample, revealing its highly heterogeneous and rough surface morphology with non-uniform pore distribution, attributed to the chemical–thermal activation process. This irregular and porous structure suggests a high density of active sites, which correlates with enhanced adsorption capacity. The EDS results confirm high carbon and oxygen content, indicative of successful activation. The detected sulfur (0.69 wt %) is attributed to the intrinsic elemental composition of the cocoa bean husks, which naturally contain minor amounts of sulfur-bearing organic compounds, such as sulfur-containing amino acids and other biomolecules. Comparable results have been documented in previous studies, where elemental analyses of cocoa husks revealed the presence of sulfur as part of their natural mineral profile [25]. These sulfur functionalities may function as polar sites, potentially enhancing the adsorption of dye molecules through electrostatic attraction or specific interactions.





	EDS
C	78.46 wt %
H	1.10 wt %
N	0.76 wt %
S	0.69 wt %
O	18.99 wt %

Figure 1. The SEM-EDS images of the CH sample.

3.2. Structural Analysis

Raman spectroscopy (Figure 2) was employed to characterize the carbon structure of the synthesized CH material. The spectrum displays two prominent features at around 1328 cm^{-1} and 1600 cm^{-1}, attributed to the D band, associated with structural defects, and the G band, characteristic of ordered graphitic domains, respectively [26]. The simultaneous presence of these bands indicates that the carbon framework contains both well-organized and defect-rich graphitic regions. The intensity ratio I_D/I_G, used here as an indicator of oxidation-related disorder in the carbon lattice [27], was determined to be approximately 1.03. This value suggests a relatively high defect density, consistent with partial oxidation and a predominantly amorphous characteristic of the material. In addition to the G and D bands, a weaker peak was observed at approximately 2500 cm^{-1}. This feature is likely related to an overtone or combination mode commonly reported in carbon-based materials, sometimes referred to as the 2D region. Its presence may indicate structural ordering effects in certain graphitic domains, as noted in previous studies [28].

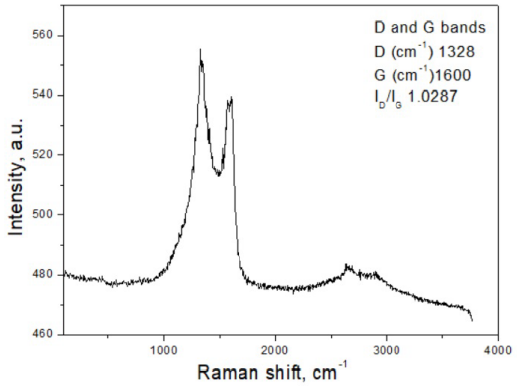


Figure 2. Raman spectrum of CH.

X-ray photoelectron spectroscopy (XPS) was employed to identify the presence of oxygen-containing functionalities on the active carbon surface. The results are presented in Table 1.

Table 1. Atomic percentages (%Atom Conc) of surface groups based on the XPS analysis from active carbon CH (C1s, O1s).

Sample		**CH**
	BE, eV	% At Conc.
C 1s		
C-C (sp^3) C=O	284.57 289.88	86.15 4.27
Total C %At Conc		90.42
O 1s		
C=O quinone type O-C=O C=O	530.54 531.96 533.46	0.19 3.28 3.83
Total O %At Conc		7.30
Total of S, N, Mn, Fe, %At Conc		2.29

The XP spectra of C1s for cocoa husk-derived activated carbon showed peaks at binding energies 284.57 and 289.88 eV, which are assigned to sp^3 hybridized carbon (C–C) and carbon from carbonyl (C=O) groups, respectively (Figure S3). The XPS C1s spectrum showed a high amount of carbon functionalities (total C % At Conc 90.42%). The O1s patterns of active carbon CH show atomic percent for oxygen functionalities, total O %At Conc about 7.3% on the surface, that indicates surface oxidation. The O1s XPS spectra of the samples (Figure S4) exhibited three main peaks with binding energies of around 530, 532 and 533 eV which correspond to the functional groups of C=O quinone type, O-C=O and C=O double bonds in carbonyl groups accordingly [29]. The proportions of them are 0.19%; 3.28% and 3.83%, respectively (Table 1). The results prove that chemical activation results in an increased presence of oxygen-containing functional groups on the surface of the activated carbon, which can enhance its adsorption properties.

3.3. Textural Properties

The BET analysis (Table 2 and Figure 3) was conducted to evaluate the surface characteristics of the synthesized adsorbent. According to the data in Table 2, the surface area of CH measures 1661.6 $m^2 \cdot g^{-1}$. Additionally, the total pore volume of active carbon is 1.5240 $cm^3 \cdot g^{-1}$, indicating that meso- and micropores dominate the structure of the material.

Table 2. Textural properties of CH: surface area and pore volume distribution.

Characteristics	Value
Total pore volume, $cm^3 \cdot g^{-1}$	1.5240
Micropore volume, $cm^3 \cdot g^{-1}$	0.5050
Mesopore volume, $cm^3 \cdot g^{-1}$	0.7498
Macropore volume, $cm^3 \cdot g^{-1}$	0.2692
BET specific surface area, $m^2 \cdot g^{-1}$	1661.6

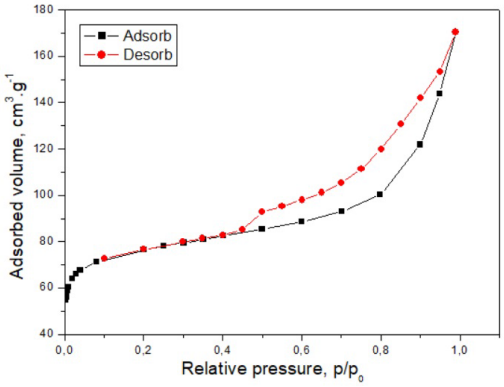


Figure 3. Adsorption–desorption isotherm of N_2 on the CH.

Figure 3 shows the results of low-temperature nitrogen adsorption–desorption measurements.

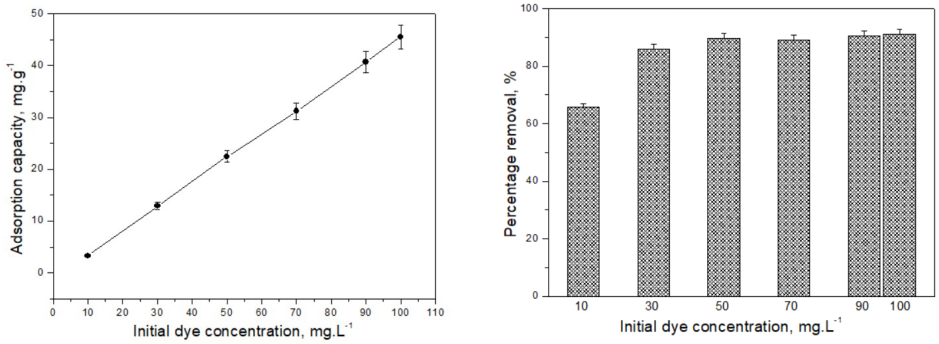
The nitrogen adsorption–desorption profile of the CH sample, recorded at 77 K (Figure 3), exhibits a type IV profile with an H4-type hysteresis loop, a feature typically associated with mesoporous solids [30]. The observed hysteresis arises from capillary condensation within mesopores as the relative pressure increases. At low relative pressures, the uptake pattern resembles that of macro porous materials, where adsorption initially proceeds via monolayer coverage of the surface. With increasing pressure, multilayer formation occurs, and once a critical threshold is reached, capillary condensation causes a pronounced rise in the adsorbed volume. After mesopore filling is complete, further adsorption is limited to the external surface area. The H4 loop shape is linked to narrow, slit-shaped pores, consistent with the pore structure inferred for the CH material.

4. Adsorption Performance

4.1. Effect of Initial Dye Concentration

To evaluate the adsorption isotherm, a series of batch experiments was conducted using CH at varying initial pollutant concentrations between 10 and 100 $mg \cdot L^{-1}$. The resulting data, presented in Figure 4, illustrate (a) the adsorption capacity of the material and (b) the corresponding removal efficiency across the tested concentration range.

The outcomes indicate that the adsorption capacity of the material increases with rising initial dye concentration in the aqueous solution, reaching a maximum value of 45.5 $mg \cdot g^{-1}$ at the highest tested concentration. Simultaneously, the purification efficiency also improves, showing a strong dependency of the adsorption process on the initial dye concentration. At lower concentrations, the ratio between dye molecules and active adsorption sites is relatively low, resulting in minimal interaction and negligible influence of concentration on the overall adsorption. However, as the concentration increases, more dye molecules encounter and bind to the available active sites, leading to enhanced adsorption capacity. Nevertheless, beyond a certain concentration threshold, the number of available active sites decreases, limiting further adsorption and consequently reducing the overall uptake efficiency.



(**a**) (**b**)

Figure 4. Dependence of adsorption capacity (**a**) and percentage purification (**b**) on the initial concentration of the pollutant in the solution.

4.2. Adsorption Isotherm Models

The maximum purification efficiency of the aqueous solution from Drimaren Red dye is expressed by the adsorption capacity of the material at equilibrium. The experimental adsorption isotherm for CH, illustrating this relationship, is presented in Figure 5.

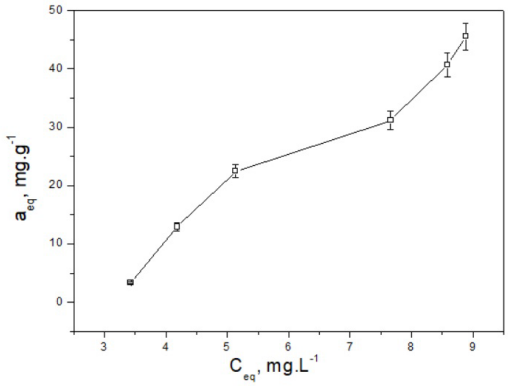


Figure 5. Equilibrium relationship between dye concentration and adsorption capacity.

The most commonly used adsorption isotherm equations that describe the relationship $a_{eq} = f(C_{eq})$ are Langmuir, Freundlich, and Dubinin–Radushkevich isotherms (Equations (3)–(5)).

$$\frac{C_{eq}}{a_{eq}} = \frac{1}{K_L \cdot a_\infty} + \frac{C_{eq}}{a_\infty} \tag{3}$$

where C_{eq} is the concentration of the dye in the solution at equilibrium, mg·L^{-1}; a_{eq} is the sorption capacity at equilibrium, mg·g^{-1}; a_∞ is the maximum sorption capacity required to form a monolayer on the adsorbent surface, mg·g^{-1}; K_L is the Langmuir constant L·mg^{-1}, which is related to the adsorption energy.

$$log a_{eq} = log K_F + (1/n) * log C_{eq} \tag{4}$$

where K_F is the Freundlich isotherm constant, mg·g^{-1}; $1/n$ is a function of the adsorption strength.

$$ln a_{eq} = ln a_\infty - K_{ad} * \varepsilon^2 \tag{5}$$

where a_{eq} and a_∞ are the equilibrium and theoretical capacities (mg·g^{-1}), K_{ad} is a constant related to adsorption energy, mol^2·kJ^{-2}; and ε is the Polanyi potential. For liquid-phase adsorption, ε was defined as:

$$\varepsilon = RT \ln\left(1 + \frac{1}{C_e}\right) \tag{6}$$

where R = 8.314 × 10^{-3} kJ·mol^{-1}K^{-1}, T is temperature (K), and C_e is the dimensionless equilibrium concentration obtained by dividing the molar C_e by the standard state (1 mol·L^{-1}). The mean adsorption energy was calculated as:

$$E = \frac{1}{\sqrt{2K_{ad}}} \quad (7)$$

and is reported in kJ·mol^{-1}.

Although originally developed for gas-phase adsorption, the Dubinin–Radushkevich model is widely used as an empirical energetic descriptor for liquid-phase adsorption on micro/mesoporous activated carbons; thus, E is interpreted as indicative under these assumptions.

The experimental results for the adsorption of Drimaren Red dye from aqueous solution with the obtained adsorbent were applied to the above-mentioned theoretical isotherms. The complete fitting plots for the Langmuir, Freundlich, and Dubinin–Radushkevich models are provided in Figure S1 (Supplementary Information), illustrating the agreement between the experimental data and the theoretical curves. The values of the coefficients and constants of the adsorption isotherms, as well as the values of the linear regression coefficients, are presented in Table 3.

Table 3. The constants and measured factors of Langmuir, Freundlich, and Dubinin–Radushkevich isotherm models for CH adsorbent.

Langmuir	Freundlich	Dubinin–Radushkevich
a_{∞}, mg·g^{-1} 10.47	K_F, mg·g^{-1} 0.3445	a_{∞}, mg·g^{-1} 73.59
K_L, L·mg^{-1} 1.133	n 0.4406	K_{ad}, mol^2·kJ^{-2} 7.38 × 10^{-3}
R_L 0.008–0.08	$1/n$ 2.26977	E, kJ·mol^{-1} 8.23
R^2 0.46	R^2 0.86	R^2 0.96

The value of the adsorption intensity parameter ($n < 1$) calculated using the Freundlich isotherm indicates cooperative adsorption behavior, particularly at low adsorbate concentrations, in agreement with observations reported by Chiban et al. [31] for biosorbents with heterogeneous surfaces. Furthermore, the heterogeneity parameter ($1/n > 1$) reinforces this cooperative effect [32], which may arise due to interactions among adsorbed molecules or the presence of energetically diverse active sites. The calculated mean free energy of adsorption (E = 8.23 kJ·mol^{-1}) derived from the Dubinin–Radushkevich isotherm falls at the lower boundary of the 8–16 kJ·mol^{-1} range, suggesting that specific surface interactions such as hydrogen bonding or ion exchange may contribute to the adsorption process, rather than dominant chemisorption. Among the tested isotherms, the Dubinin–Radushkevich model provided the best fit to the experimental data, as evidenced by a high correlation coefficient ($R^2 > 0.9$) and low standard deviation. These results suggest that the adsorption of Drimaren Red dye onto the cocoa husk-based carbon adsorbent is most accurately described by a model incorporating energetic heterogeneity and specific surface interactions.

4.3. Kinetic Models

To evaluate the adsorption process from its onset until equilibrium was reached, experiments were conducted at different temperatures (20 °C and 40 °C) and contact times ranging from 1 to 25 min, using an initial dye concentration of 100 mg·L^{-1} (Figure 6).

During the adsorption process using the CH adsorbent at 20 °C, a rapid adsorption phase was observed within the first five minutes, followed by a slower increase in the amount of dye adsorbed. By increasing the temperature to 40 °C, the process proceeds significantly more intensively, reaching a dye removal efficiency of approximately 93% by the third minute. However, with extended contact time, a decrease in the amount adsorbed was recorded, decreasing to approximately 89% by the 25th minute. These results

highlight the substantial influence of temperature on the adsorption efficiency of Drimaren Red dye when using the CH adsorbent. The decline in the amount of dye adsorbed after the third minute was likely due to hydrodynamic factors related to stirring, which may induce desorption of some physically adsorbed dye molecules. The faster initial uptake at 40 °C was attributed to the lower viscosity of water and partial disaggregation of Drimaren Red molecules, reducing their effective hydrodynamic radius and enhancing diffusion into the micro-/mesoporous slit-like channels of the CH adsorbent. At extended contact times, increased thermal energy may facilitate desorption of weakly bound molecules and hinder the formation of multilayer structures on external surfaces, thereby slightly lowering adsorption capacity.

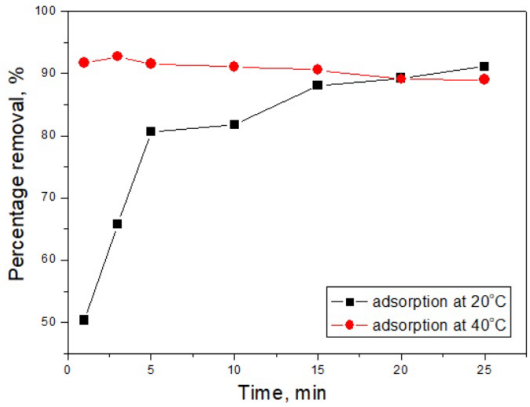


Figure 6. Percentage of dye removal as a function of contact time.

A more accurate characterization of the adsorption kinetics over time and at different temperatures was performed by applying models such as the pseudo-first order (Equation (8)), pseudo-second order (Equation (9)), and the Weber–Morris intraparticle diffusion model (Equation (10)). The full fitting plots for the kinetic models are presented in Figure S2 (Supplementary Information), depicting the adsorption dynamics at different temperatures.

$$\frac{dq_t}{dt} = k_L(q_e - q_t) \tag{8}$$

$$\frac{t}{q_t} = \left(\frac{1}{k_2 {q_e}^2}\right) + \left(\frac{t}{q_e}\right) \tag{9}$$

$$q_t = k_i t_{1/2} + C \tag{10}$$

where q_e and q_t represent the amounts of sorbate adsorbed onto the material at equilibrium and at time t (min), respectively; k_L (min^{-1}), k_2 ($\text{g}\cdot\text{mg}^{-1}\cdot\text{min}^{-1}$), and k_i ($\text{mg}\cdot\text{g}^{-1}\cdot\text{min}^{-1}$) are the rate constants of the pseudo-first-order, pseudo-second-order, and Weber–Morris kinetic models, respectively. The constant C is related to the boundary layer thickness and may also reflect structural factors, such as interlayer connectivity within the adsorbent.

Table 4 presents the kinetic parameters for Drimaren Red K-7B adsorption onto cocoa husk-derived activated carbon. The process followed the pseudo-second-order model, with R^2 = 0.99 at both 20 °C and 40 °C. Although this model is often linked to chemisorption [33], XPS analysis revealed oxygen-containing groups (e.g., carbonyl, carboxyl) that favor hydrogen bonding and polar interactions. These findings indicate that physisorption and surface-mediated interactions dominate, rather than valence-level electron exchange. Thus, the model reflects the overall kinetic behavior without confirming chemisorption as the dominant mechanism. The rate constant (k_2) showed a substantial increase from 0.0204 to 0.192 $\text{g}\cdot\text{mg}^{-1}\cdot\text{min}^{-1}$ with rising temperature, suggesting that the adsorption process is thermally activated. Despite this, the equilibrium adsorption capacity

($q_e \approx 45$ mg·g^{-1}) remained relatively constant, indicating thermal stability of the active sites and minimal structural deterioration within the adsorbent matrix. Although the pseudo-first-order model yielded a marginally higher R^2 at 40 °C compared to 20 °C, the calculated q_e (0.45 mg·g^{-1}) was drastically lower than the experimental value (~44.6 mg·g^{-1}). This severe underestimation demonstrates that the model cannot adequately describe the adsorption process under the studied conditions, a limitation also noted in similar biosorbent studies [34]. The intraparticle diffusion model revealed higher intercepts (C) at elevated temperature, indicating that intraparticle diffusion contributes but is not the sole rate-limiting step; the increased C suggests a thicker boundary layer and multi-stage transport under the studied conditions [35]. Given that all experiments were conducted under batch mode with continuous agitation, external mass transfer resistance is assumed negligible. Therefore, the rate-limiting step appears to be governed predominantly by surface interactions and intraparticle transport processes, acting in tandem to ensure rapid and efficient dye uptake.

Table 4. Calculated parameters of the applied kinetic models.

T, °C	Pseudo-First-Order			Pseudo-Second-Order			Weber–Morris		
	R^2	k_1 min^{-1}	q_e mg·g^{-1}	R^2	k_2 g·mg^{-1}·min^{-1}	q_e mg·g^{-1}	R^2	k_i mg·g^{-1}·min^{-1}	C
20	0.95	0.156	18.6	0.99	0.0204	46.79	0.84	5.2	23.6
40	0.96	0.064	0.45	0.99	0.192	44.58	0.74	0.4	46.65

For comparison, Table 5 summarizes the adsorption performance of CH and various dye adsorbents reported in the literature under comparable conditions.

Table 5. Comparative adsorption performance of various adsorbents for dye removal.

Adsorbent Material	BET (m^2·g^{-1})	Adsorption Capacity (mg·g^{-1})	Time, min	Removal	Adsorbate (Dye)	Reference
CH	**1661**	**45.5**	**3**	**93%**	**Drimaren Red K-7B**	**This work**
Banana peel powder	118	49	90	Not specified	Reactive Black 5	[36]
Coconut shell ACF	1556	21.3	120–150 min	>90% (varies)	Methylene blue	[29]
Coconut shell ACF	1556	22.1	120–150 min	>90% (varies)	Congo red	[29]
Orange peel AC	512.2	111.1	60 min	~100%	Methyl red	[37]

As shown in Table 5, the cocoa husk-derived activated carbon demonstrates a notably high specific surface area and excellent adsorption performance. Even at a short contact time, CH achieves high dye removal efficiency and adsorption capacity, showing performance comparable to or exceeding that of the adsorbents reported in the cited studies. This combination of rapid uptake and high efficiency reflects the synergistic effect of the material's large surface area, well-developed micro/mesoporous structure, and favorable surface chemistry. These characteristics highlight CH as a competitive option for fast and effective dye removal under conditions relevant to real wastewater treatment scenarios.

5. Thermodynamic Studies

Equilibrium data from the kinetic experiments at 20 °C (293.15 K) and 40 °C (313.15 K) were used to evaluate the thermodynamic parameters of the adsorption process. The experiments were performed with an initial dye concentration C_0 = 100 mg·L^{-1}, solution volume V = 12.5 mL, and adsorbent mass m = 0.025 g. The equilibrium adsorption capacities obtained from the kinetic study were q_e = 46.79 mg·g^{-1} at 20 °C and q_e = 44.58 mg·g^{-1} at 40 °C. Equilibrium concentrations (C_e) were calculated from the mass balance equation:

$$C_e = C_o - \frac{q_e * m}{V} \quad (11)$$

The dimensionless equilibrium constant for batch systems was defined as:

$$K = \frac{C_o - C_e}{C_e} \quad (12)$$

The calculated K values were 14.58 for 20 °C and 8.23 for 40 °C. The standard Gibbs free energy change (ΔG°) was determined using:

$$\Delta G^o = -RT\ln K \quad (13)$$

where $R = 8.314\ \mathrm{J\cdot mol^{-1}\cdot K^{-1}}$. The enthalpy ($\Delta H^\circ$) and entropy ($\Delta S^\circ$) changes were obtained from the van't Hoff equation [27]:

$$\ln K = \frac{\Delta S^o}{R} - \frac{\Delta H^o}{R}\frac{1}{T} \quad (14)$$

A linear fit of ln$K$ versus $1/T$ yielded $\Delta H^\circ = -21.9\ \mathrm{kJ\cdot mol^{-1}}$ and $\Delta S^\circ = -52.4\ \mathrm{J\cdot mol^{-1}\cdot K^{-1}}$. Table 6 summarizes the thermodynamic parameters.

Table 6. Thermodynamic parameters for the adsorption of Drimaren Red onto CH carbon adsorbent.

Temperature (K)	K	ΔG° (kJ·mol^{-1})	ΔH° (kJ·mol^{-1})	ΔS° (J·mol^{-1}·K^{-1})
293.15 (20 °C)	14.58	−6.53		
313.15 (40 °C)	8.23	−5.49	−21.9	−52.4

Negative ΔG° values at both temperatures confirm the spontaneous nature of the adsorption process. The process is exothermic with $\Delta H^\circ = -21.9\ \mathrm{kJ\cdot mol^{-1}}$ and accompanied by a negative entropy change ($\Delta S^\circ = -52.4\ \mathrm{J\cdot mol^{-1}\cdot K^{-1}}$), indicating increased ordering at the solid–liquid interface during adsorption. The decrease of K with increasing temperature corroborates the exothermic character.

6. Working Hypotheses for Adsorption Analysis

The integrated characterization points to a heterogeneous, oxygen-functionalized carbon surface with a high specific area and slit-like micro/mesopores, as evidenced by SEM-EDS, Raman ($I_D/I_G \approx 1.03$), BET (1661.6 $\mathrm{m^2\cdot g^{-1}}$), and the type IV (H4) N_2 isotherm [33]. These features support rapid external adsorption followed by intraparticle diffusion. The kinetic data fit the pseudo-second-order model ($R^2 = 0.99$) at both 20 °C and 40 °C, indicating that the overall rate is governed by surface interactions [33], while the pronounced increase of k_2 with temperature reflects thermally enhanced mass transfer and pore diffusion. The Weber–Morris analysis (increasing intercept C with T) further corroborates the growing contribution of intraparticle transport at elevated temperature [38].

Isotherm analysis reveals energetic heterogeneity and cooperative uptake: the Dubinin–Radushkevich model provides the best fit ($R^2 = 0.96$) with $E = 8.23\ \mathrm{kJ\cdot mol^{-1}}$, pointing to specific surface-mediated interactions superimposed on physisorption [39]. The Freundlich parameters ($n = 0.4406 < 1$, $1/n = 2.26977 > 1$) indicate cooperative adsorption on a heterogeneous surface, especially pronounced at low concentrations, consistent with interactions among adsorbed molecules and energetic site diversity [40]. Thermodynamically, the process is spontaneous at both studied temperatures ($\Delta G^\circ = -6.53$ and $-5.49\ \mathrm{kJ\cdot mol^{-1}}$ at 293 and 313 K, respectively), exothermic ($\Delta H^\circ = -21.9\ \mathrm{kJ\cdot mol^{-1}}$), and accompanied by a more pronounced decrease in interfacial entropy ($\Delta S^\circ = -52.4\ \mathrm{J\cdot mol^{-1}\cdot K^{-1}}$) [41], consistent with significant ordering at the solid-liquid interface during dye binding. The decrease in the equilibrium constant with temperature aligns with exothermic adsorption, whereas

the faster early-time removal at 40 °C is attributed to improved diffusion and reduced solution viscosity.

In addition to the kinetic, isotherm, and thermodynamic evidence supporting a two-stage adsorption process—rapid surface uptake followed by slower intraparticle diffusion—the surface chemistry of the CH material provides further insight into the mechanism. XPS analysis revealed the presence of oxygen-containing functionalities, including carbonyl and carboxyl groups, generated during chemical activation. These polar sites are likely to engage in hydrogen bonds and electrostatic associations with dye molecules, complementing the physisorption and pore-filling processes inferred from the modeling results. The coexistence of such chemical interactions with textural effects supports the view that adsorption proceeds through a combination of physical and specific surface-mediated mechanisms.

7. Conclusions

Cocoa husks were successfully transformed into high-performance activated carbon through carbonization followed by KOH activation. The resulting adsorbent exhibits an exceptionally high specific surface area (1661.6 $m^2 \cdot g^{-1}$), substantial total pore volume (1.5240 $cm^3 \cdot g^{-1}$), and a micro/mesoporous architecture with slit-like pores. Under an initial dye concentration of 100 $mg \cdot L^{-1}$, CH achieved over 90 % removal of Drimaren Red K-7B within three minutes at 40 °C, with equilibrium capacities of ~45–47 $mg \cdot g^{-1}$. Kinetic analysis confirmed pseudo-second-order behavior with temperature-enhanced rate constants, while isotherm fitting favored the Dubinin–Radushkevich model (E = 8.23 $kJ \cdot mol^{-1}$), indicating specific surface-mediated interactions on a heterogeneous surface. Thermodynamic evaluation revealed a spontaneous process at both studied temperatures ($\Delta G^\circ = -6.53$ and -5.49 $kJ \cdot mol^{-1}$), distinctly exothermic ($\Delta H^\circ = -21.9$ $kJ \cdot mol^{-1}$), and accompanied by a more pronounced negative entropy change ($\Delta S^\circ = -52.4$ $J \cdot mol^{-1} \cdot K^{-1}$), consistent with significant ordering at the solid–liquid interface during dye binding. The decrease in equilibrium constant with temperature aligns with the exothermic nature of adsorption, while the faster initial uptake at higher temperature is attributed to improved diffusion and reduced solution viscosity. XPS characterization further confirmed the presence of oxygen-bearing functional groups on the carbon surface, including carbonyl and carboxyl moieties, which enhance the material's affinity toward dye molecules through polar and hydrogen-bonding interactions. This surface chemistry acts synergistically with the high surface area and hierarchical pore structure to promote efficient adsorption. These combined features—rapid kinetics, high equilibrium performance, and the sustainable, low-cost nature of the precursor—position cocoa husk-derived activated carbon as an efficient and eco-friendly adsorbent for wastewater treatment, contributing to resource valorization and circular economy goals. Future work will extend these promising results by validating the performance of the cocoa husk-derived activated carbon in real wastewater systems, further strengthening its potential for sustainable water treatment applications.

Supplementary Materials: The following supporting information can be downloaded at: https://www.mdpi.com/article/10.3390/separations12100278/s1, Figure S1: Fitting plots of Langmuir (a), Freundlich (b), and Dubinin–Radushkevich (c) isotherms for dye adsorption onto CH; Figure S2: Fitting plots of pseudo-first-order (a), pseudo-second-order (b), and Weber–Morris (c) kinetic models for dye adsorption onto CH; Figure S3: X-ray photoelectron spectroscopy (XPS) of the C1s binding energy (284.57 and 289.88 eV) of cocoa husk–derived activated carbon; Figure S4: X-ray photoelectron spectroscopy (XPS) of the O1s binding energy (530.54; 531.96 and 533.46 eV) of cocoa husk–derived activated carbon.

Author Contributions: Conceptualization, D.A., V.T. and G.G.; methodology, D.A. and G.G.; software, D.A. and G.G.; validation, D.A., V.T. and G.G.; formal analysis, D.A. and G.G.; investigation, D.A.; data curation, D.A.; writing—original draft preparation, D.A.; writing—review and editing, D.A. and V.T.; visualization, D.A. and G.G.; supervision, D.A. and V.T.; project administration, D.A. All authors have read and agreed to the published version of the manuscript.

Funding: This research was funded by the European Union's NextGenerationEU, through the National Recovery and Resilience Plan of the Republic of Bulgaria, project № BG-RRP-2.004-0002, "BiOrgaMCT".

Data Availability Statement: The original contributions presented in this study are included in the article/Supplementary Materials. Further inquiries can be directed to the corresponding author.

Conflicts of Interest: The authors declare no conflicts of interest.

References

1. Yu, D.; Wang, L.; Wu, M. Simultaneous removal of dye and heavy metal by banana peels derived hierarchically porous carbons. *J. Taiwan Inst. Chem. Eng.* **2018**, *93*, 543–553. [CrossRef]
2. UNESCO World Water Assessment Programme (WWAP). *The United Nations World Water Development Report 2017: Wastewater, the Untapped Resource*; UNESCO: Paris, France, 2017. Available online: https://www.unesco.org/en/wwap/wwdr/2017 (accessed on 31 August 2025).
3. Hashem, A.H.; Saied, E.; Hasanin, M.S. Green and ecofriendly bio-removal of methylene blue dye from aqueous solution using biologically activated banana peel waste. *Sustain. Chem. Pharm.* **2020**, *18*, 100333. [CrossRef]
4. Chanikya, P.; Nidheesh, P.V.; Babu, D.S.; Gopinath, A.; Kumar, M.S. Treatment of dyeing wastewater by combined sulfate radical based electrochemical advanced oxidation and electrocoagulation processes. *Sep. Purif. Technol.* **2021**, *254*, 117570. [CrossRef]
5. Xue, Y.; Liu, X.; Zhang, N.; Shao, Y.; Xu, C.C. Enhanced photocatalytic performance of iron oxides@HTCC fabricated from zinc extraction tailings for methylene blue degradation. *Metall. Mater.* **2023**, *30*, 2364–2374.
6. Lu, C.; Yang, J.; Khan, A.; Yang, J.; Li, Q.; Wang, G. A highly efficient technique to simultaneously remove acidic and basic dyes using magnetic ion-exchange microbeads. *J. Hazard. Mater.* **2022**, *304*, 114173. [CrossRef]
7. Khapre, M.A.; Pandey, S.; Jugade, R.M. Glutaraldehyde-cross-linked chitosan–alginate composite for organic dyes removal from aqueous solutions. *Int. J. Biol. Macromol.* **2021**, *190*, 862–875. [CrossRef]
8. Gupta, R.; Pandit, C.; Pandit, S.; Gupta, P.K.; Lahiri, D.; Agarwal, D.; Pandey, S. Potential and future prospects of biochar-based materials and their applications in removal of organic contaminants from industrial wastewater. *J. Mater. Cycles Waste Manag.* **2022**, *24*, 852–876. [CrossRef]
9. Subrahmanya, T.; Widakdo, J.; Mani, S.; Austria, H.F.M.; Hung, W.-S.; Makari, H.; Nagar, J.K.; Hu, C.-C.; Lai, J.-Y. An eco-friendly and reusable syringe filter membrane for the efficient removal of dyes from water via low pressure filtration assisted self-assembling of graphene oxide and SBA-15/PDA. *J. Hazard. Mater.* **2022**, *349*, 131425. [CrossRef]
10. Shen, Y.; Sun, P.; Ye, L.; Xu, D. Progress of anaerobic membrane bioreactor in municipal wastewater treatment. *Sustainability* **2023**, *15*, 1277–1298. [CrossRef]
11. Toteva, V.; Staneva, D.; Grabchev, I. Pollutants sorbent made of cotton fabric modified with chitosan-glutaraldehyde and zinc oxide particles. *Materials* **2021**, *14*, 3242. [CrossRef]
12. Rehman, R.; Farooq, S.; Mahmud, T. Use of agro-waste Musa acuminata and Solanum tuberosum peels for economical sorptive removal of emerald green dye in ecofriendly way. *J. Clean. Prod.* **2019**, *206*, 819–826. [CrossRef]
13. Khapre, M.; Shekhawat, A.; Saravanan, D.; Pandey, S.; Jugade, R. Mesoporous Fe-Al-doped cellulose for the efficient removal of reactive dyes. *Mater. Adv.* **2022**, *3*, 3278–3285. [CrossRef]
14. Rondina, D.J.G.; Ymbong, D.V.; Cadutdut, M.J.M.; Nalasa, J.R.S.; Paradero, J.B.; Mabayo, V.I.F.; Arazo, R.O. Utilization of a novel activated carbon adsorbent from press mud of sugarcane industry for the optimized removal of methyl orange dye in aqueous solution. *Appl. Water Sci.* **2019**, *9*, 181. [CrossRef]
15. Pandey, S.; Son, N.; Kang, M. Synergistic sorption performance of karaya gumrosslink poly(acrylamide-co-acrylonitrile)@metal nanoparticle for organic pollutants. *Int. J. Biol. Macromol.* **2022**, *210*, 300–314. [CrossRef]
16. Ouyang, M.; Wang, B.; Yu, X.; Tang, W.; Yu, M.; You, C.; Yang, J.; Wang, T.; Deng, Z. Comparative study on full-scale pore structure characterization and gas adsorption capacity of shale and coal reservoirs. *Processes* **2025**, *13*, 2246. [CrossRef]
17. Akhtar, M.S.; Ali, S.; Zaman, W. Innovative adsorbents for pollutant removal: Exploring the latest research and applications. *Molecules* **2024**, *29*, 4317. [CrossRef]
18. Zhang, J.; Wang, Y.; Liang, D.; Xiao, Z.; Xie, Y.; Li, J. Sulfhydryl-Modified Chitosan Aerogel for the Adsorption of Heavy Metal Ions and Organic Dyes. *Ind. Eng. Chem. Res.* **2020**, *59*, 14531–14536. [CrossRef]

19. Goyal, A.; Singh, P.; Chamoli, P.; Raina, K.K.; Shukla, R.K. Eco-Friendly Biowaste-Based Natural Surfactant for Lyotropic Assemblies and Bio-Adsorbent for Dye Removal. *Inorg. Chem. Commun.* **2021**, *133*, 108871. [CrossRef]
20. Kloster, M.; Marcovich, N.E.; Mosiewicki, M.A. Microcrystalline Cellulose Modified Chitosan Aerogels to Enhance Congo Red Dye Adsorption. *Colloids Surf. A Physicochem. Eng. Asp.* **2025**, *707*, 135823. [CrossRef]
21. Stanciu, M.-C.; Teacă, C.-A. Natural Polysaccharide-Based Hydrogels Used for Dye Removal. *Gels* **2024**, *10*, 243. [CrossRef]
22. Mihai, S.; Bondarev, A.; Necula, M. The Potential of Biogenic Materials as Sustainable and Environmentally Benign Alternatives to Conventional Adsorbents for Dyes Removal: A Review. *Processes* **2025**, *13*, 589. [CrossRef]
23. Recio-Colmenares, C.L.; Flores-Gómez, J.; Morales Rivera, J.P.; Palacios Hinestroza, H.; Sulbarán-Rangel, B. Green Materials for Water and Wastewater Treatment: Mechanisms and Artificial Intelligence. *Processes* **2025**, *13*, 566. [CrossRef]
24. Tran, H.N. Adsorption technology for water and wastewater treatments. *Water* **2023**, *15*, 2857. [CrossRef]
25. Soares, T.F.; Oliveira, M.B.P.P. Cocoa By-Products: Characterization of Bioactive Compounds and Beneficial Health Effects. *Molecules* **2022**, *27*, 1625. [CrossRef]
26. Pan, T.; Guo, Z.; Zhang, X.; Feng, L. Hydrothermal carbonization of biomass waste and application of produced hydrochar in organic pollutants removal. *J. Clean. Prod.* **2024**, *457*, 142386. [CrossRef]
27. Yin, Q.; Zhang, B.; Wang, R.; Zhao, Z. Biochar as an adsorbent for inorganic nitrogen and phosphorus removal from water: A review. *Environ. Sci. Pollut. Res.* **2017**, *24*, 26297–26309. [CrossRef]
28. Ferrari, A.C.; Robertson, J. Interpretation of Raman spectra of disordered and amorphous carbon. *Phys. Rev. B* **2000**, *61*, 14095–14107. [CrossRef]
29. Zhang, L.; Tu, L.-Y.; Liang, Y.; Chen, Q.; Li, Z.-S.; Li, C.-H.; Wang, Z.-H.; Li, W. Coconut-based activated carbon fibers for efficient adsorption of various organic dyes. *RSC Adv.* **2018**, *8*, 42280–42291. [CrossRef]
30. Yurdakal, S.; Garlisi, C.; Özcan, L.; Bellardita, M.; Palmisano, G. (Photo)catalyst characterization techniques: Adsorption isotherms and BET, SEM, FTIR, UV Vis, photoluminescence, and electrochemical characterizations. In *Heterogeneous Photocatalysis: Relationships with Heterogeneous Catalysis and Perspectives*; Marci, G., Palmisano, L., Eds.; Elsevier: Amsterdam, The Netherlands, 2019; Chapter 4. [CrossRef]
31. Chiban, M.; Soudani, A.; Sinan, F.; Persin, M. Single, binary and multi-component adsorption of some anions and heavy metals on environmentally friendly *Carpobrotus edulis* plant. *Colloids Surf. B Biointerfaces* **2011**, *82*, 267–276. [CrossRef]
32. Voudrias, E.; Fytianos, F.; Bozani, E. Sorption desorption isotherms of dyes from aqueous solutions and wastewaters with different sorbent materials. *Glob. Nest Int. J.* **2002**, *4*, 75–83.
33. Abubakar, U.I.; Abdullahi, M.; Abdulhamid, H. Kinetics, equilibrium, and thermodynamics studies of Methylene Blue dye adsorption onto modified activated carbon produced from groundnut shells. *J. Mater. Environ. Sci.* **2024**, *15*, 893–915.
34. Simonin, J.-P. On the comparison of pseudo-first order and pseudo-second order rate laws in the modeling of adsorption kinetics. *Chem. Eng. J.* **2016**, *300*, 254–263. [CrossRef]
35. El-Sayed, M.; Abukhadra, M.R.; Rabie, R.; Shawky, A. Efficient removal of methylene blue dye using novel biochar derived from palm leaves: Characterization, equilibrium isotherms, and kinetic modeling. *Separations* **2023**, *10*, 211. [CrossRef]
36. Munagapatia, V.S.; Wen, J.-C.; Pan, C.-L.; Gu, Y.; Wen, J.-H.; Reddy, G.M. Adsorptive removal of anionic dye (Reactive Black 5) from aqueous solution using chemically modified banana peel powder: Kinetic, isotherm, thermodynamic, and reusability studies. *Int. J. Phytoremediat.* **2020**, *22*, 267–278. [CrossRef] [PubMed]
37. Deshmukh, S.; Topare, N.S.; Raut-Jadhav, S.; Thorat, P.V.; Bokil, S.A.; Khan, A. Orange peel activated carbon produced from waste orange peels for adsorption of methyl red. *AQUA Water Infrastruct. Ecosyst. Soc.* **2022**, *71*, 1351–1363. [CrossRef]
38. Yahaya, N.F.; Aziz, H.A.; Adlan, M.N.; Ariffin, M. Adsorption of copper by *Pycnoporus sanguineus* biomass: Isotherm and thermodynamic studies. *J. Environ. Chem. Eng.* **2015**, *3*, 2161–2169. [CrossRef]
39. Sahmoune, M.N. Evaluation of thermodynamic parameters for adsorption of heavy metals by green adsorbents. *Environ. Chem. Lett.* **2019**, *17*, 697–704. [CrossRef]
40. Vigdorowitsch, M.; Pchelintsev, A.; Tsygankova, L.; Tanygina, E. Freundlich isotherm: An adsorption model complete framework. *Appl. Sci.* **2021**, *11*, 8078. [CrossRef]
41. Nekouei, F.; Nekouei, S.; Tyagi, I.; Gupta, V. Kinetic, thermodynamic and isotherm studies for Acid Blue 129 removal from liquids using copper oxide nanoparticle-modified activated carbon as a novel adsorbent. *J. Mol. Liq.* **2015**, *201*, 124–133. [CrossRef]

Disclaimer/Publisher's Note: The statements, opinions and data contained in all publications are solely those of the individual author(s) and contributor(s) and not of MDPI and/or the editor(s). MDPI and/or the editor(s) disclaim responsibility for any injury to people or property resulting from any ideas, methods, instructions or products referred to in the content.